

Effects of Isothermal and Adiabatic Thermal Loadings on Size and Strain Rate Dependence of Copper Nanowire

Vijay Kumar Sutrakar¹ and D. Roy Mahapatra²

¹Aeronautical Development Establishment, Bangalore-560 075

²Indian Institute of Science, Bangalore-560 012

ABSTRACT

In the present paper, the size and strain rate effects on ultra-thin $\langle 100 \rangle / \{ 100 \}$ Cu nanowires at an initial temperature of 10 K have been discussed. Extensive molecular dynamics (MD) simulations have been performed using Embedded atom method (EAM) to investigate the structural behaviours and properties under high strain rate. Velocity-Verlet algorithm has been used to solve the equation of motions. Two different thermal loading cases have been considered: (i) Isothermal loading, in which Nose-Hoover thermostat is used to maintain the constant system temperature, and (ii) Adiabatic loading, i.e., without any thermostat. Five different wire cross-sections were considered ranging from $0.723 \times 0.723 \text{ nm}^2$ to $2.169 \times 2.169 \text{ nm}^2$. The strain rates used in the present study were $1 \times 10^9 \text{ s}^{-1}$, $1 \times 10^8 \text{ s}^{-1}$, and $1 \times 10^7 \text{ s}^{-1}$. The effect of strain rate on the mechanical properties of copper nanowires was analysed, which shows that elastic properties are independent of thermal loading for a given strain rate and cross-sectional dimension of nanowire. It showed a decreasing yield stress and yield strain with decreasing strain rate for a given cross-section. Also, a decreasing yield stress and increasing yield strain were observed for a given strain rate with increasing cross-sectional area. Elastic modulus was found to be $\sim 100 \text{ GPa}$, which was independent of processing temperature, strain rate, and size for a given initial temperature. Reorientation of $\langle 100 \rangle / \{ 100 \}$ square cross-sectional copper nanowires into a series of stable ultra-thin pentagon copper nanobridge structures with dia of $\sim 1 \text{ nm}$ at 10 K was observed under high strain rate tensile loading. The effect of isothermal and adiabatic loading on the formation of such pentagonal nanobridge structure has been discussed.

Keywords: Metallic nanowires, sensors, nanosystems, copper nanowires, nanobridge structure, molecular dynamics simulation, nano-electronic device fabrication, isothermal loading, thermal loading, adiabatic thermal loading.

1. INTRODUCTION

The structural properties of metallic nanowires have been extensively investigated over the past decade. Understanding of these properties is important in the context of nano-electronic device fabrications. The structures of ultra-thin nanowires of *Au*¹⁻⁶, *Cu*⁷⁻⁹, *Pb*, *Al*¹⁰⁻¹², *Ag*¹³, and *Ti*¹⁴ have been investigated using MD simulations. These studies show that helical, multi-shelled, and filled structures exist in several face-centered-cubic (FCC) metals in the form of ultra-thin nanowires. Because of the strong surface effect, unique behaviours such as surface-stress-induced phase transformation¹⁵, lattice reorientation¹⁶⁻¹⁷ have also been observed. Nanowires are of great technological importance because of their unique structures, properties, and potential applications in nanoscale electronics, photonics, biological, and chemical sensors¹⁸⁻¹⁹. In the recent years, various nano-devices have been developed from nanowires, such as nanolasers²⁰⁻²¹, Field-effect transistors (FET)²²⁻²³, light emitting diodes²⁴, and quantised conductance atomic switches²⁵. Nanowire sensors have also been fabricated for highly sensitive and selective detection of biological and chemical species such as hydrogen²⁶, CO and NO₂ gases²⁷, proteins, and DNA²⁸. These nanowires components

have even been integrated as address decoders for nanosystems such as biological sensor arrays and nanocomputers²⁹.

Among all nanowires, metal nanowires have drawn a lot of interest because of their appealing properties such as high thermal and electrical conductivity, and quantised conductance³⁰⁻³³. In the previous work on copper nanowires, atomistic simulations under various conditions have produced many different polygonal cross-section copper nanowires⁹, such as rectangular, pentagonal, and hexagonal ones. Many studies on the structures of nanowires have shown that some nano particles are related to a decahedron model, e.g., in *Ag*³⁴, *Ni*³⁴, *Au*³⁴⁻³⁷, *Cu*³⁸⁻³⁹. Mehrez and Ciraci⁴⁰ have reported the formation of hexagonal rings formed from $\{ 111 \}$ oriented *Cu* at 150 K. These hexagonal rings further transform into pentagonal rings during mechanical stretching. Sen,⁴¹ *et al* have performed an extensive first-principles study of nanowires with various pentagonal structures by using pseudo-potential plane wave method within the framework of density functional theory. They have shown that nanowires of different types of elements, such as alkali, simple, transition, and noble metals and inert gas atoms have a stable structure made of staggered pentagonal shape with a linear chain perpendicular to the planes of the pentagon and passing

through their centres. This is due to the fact that the pentagonal quasi-1-D nanowires have higher cohesive energy than many other 1-D structural arrangements. Recently, Gonzalez,⁴² *et al.* have shown by their experimental and theoretical studies that copper nanowires formed by mechanical stretching exhibit structural relaxation forming pentagonal [110] copper nanowires with a quantum conductance of $\sim 4.5 G_0$. Recently, authors have shown the formation of stable pentagonal multi-shell nanobridge structure under dynamic loading of [100]/ {100} copper nanowires⁴³ at 10 K. Under a range of high strain rate loading, such pentagonal multi-shell nanobridge structures with enhanced mechanical properties have been found. Effect of temperature, ranging from 10 K - 600 K has also been analysed under various strain rates and various cross-sectional dimensions to find the existence of pentagonal nanobridge structure^{44, 45}. In these studies, the authors have considered only the isothermal loading whereas no temperature effects during the loading process were considered, which could lead to different deformations as well as different mechanical properties under such high strain rate loading. The present paper aims at understanding the effects of adiabatic loading and strain rates on the mechanical properties of nanowires of various cross-sectional dimensions. The effect of adiabatic loading on the formation of pentagonal nanobridge structure is also discussed in detail and results are compared with those obtained due to isothermal loading.

2. SIMULATION METHOD

Molecular dynamic simulation of copper nanowires using the embedded atom method (EAM)^{46,47} as the underlying model of inter-atomic interactions has been considered. In the EAM, the total energy E for a system of atoms is written as

$$E = \sum_i F_i(\rho_i) + \frac{1}{2} \sum_{j \neq i} \phi_{ij}(r_{ij}), \quad (1)$$

where the summations in Eqn.(1) extend over the total number of atoms N in the system, F_i is the embedded function, ρ_i is the electron density at atom i , ϕ_{ij} is a pair-wise interaction function and r_{ij} is the distance between atom i and j . In this work, the EAM potential developed by Mishin⁴⁸ *et al.* is utilised, which accurately represents the elastic properties and surface energies of copper. More importantly, the potential accurately captures the stacking fault and twinning energies, which is critical in analysing inelastic deformation.

Copper nanowires with square cross-section $\langle 100 \rangle / \{100\}$ were created using known lattice parameters of a bulk FCC crystal as shown in Fig.1. The length of the nanowire was kept constant at 13 nm with five different cross-sectional dimensions of $0.723 \times 0.723 \text{ nm}^2$, $1.0845 \times 1.0845 \text{ nm}^2$, $1.446 \times 1.446 \text{ nm}^2$, $1.8075 \times 1.8075 \text{ nm}^2$, and $2.169 \times 2.169 \text{ nm}^2$ were considered for the simulation. The nanowires were first relaxed to equilibrium configurations using the conjugate gradient method; the nanowires were then thermally

equilibrated at 10 K using the Nose-Hoover thermostat^{49,50} for 10 ps with a time step of 0.001 ps before being loaded under tension along the nanowire's axis and was allowed to relax by holding the length of the nanowire unchanged. The nanowires are not relaxed to a zero stress state and the beginning of deformation was at stress level of 1.5 - 8.0 GPa. A similar procedure was also used by Liang and Zhou⁵¹ in the MD simulation during tensile deformation of copper nanowires.

Two different thermal loading conditions were considered: (i) isothermal loading, and (ii) adiabatic loading. In the case of isothermal loading, Nose-Hoover thermostat was used simultaneously with uniaxial loading for maintaining the nanowires temperature constant at 10 K during the deformation process. In the case of adiabatic loading, no thermostats were used during loading process and the temperature is allowed to evolve. The nanowires get heated up during loading which captures the realistic behavior at such high strain rates.

A uniaxial loading was performed by completely restraining one end of the wire, then by applying velocities to atoms along the loading direction that go linearly from zero at fixed-end to the maximum value at the free-end, creating a ramp velocity profile. This ramp velocity was used to avoid the emission of shock waves from the fixed-end of the nanowire. Different strain rates ranging from $1 \times 10^9 \text{ s}^{-1}$ to $1 \times 10^7 \text{ s}^{-1}$ were used for each nanowire. The equations of motion were integrated using velocity Verlet algorithm⁵². All simulations were performed using an MD code called LAMMPS^{53,54} developed by Sandia National Laboratory. No periodic boundary conditions were used at any stage of simulation, which was to capture accurately the relevant surface effects. The stresses were calculated using the virial theorem⁵⁵, which takes the form

$$\sigma_{ij} = \frac{1}{V} \left(\frac{1}{2} \sum_{\alpha=1}^N \sum_{\beta \neq \alpha}^N U'(r^{\alpha\beta}) \frac{\Delta x_i^{\alpha\beta} \Delta x_j^{\alpha\beta}}{r^{\alpha\beta}} - \sum_{\alpha=1}^N m_\alpha \dot{x}_i^\alpha \dot{x}_j^\alpha \right) \quad (2)$$

where N is the total number of atoms, $r^{\alpha\beta}$ is the distance between the two atoms α and β , $\Delta x_i^{\alpha\beta} = x_i^\alpha - x_i^\beta$, U is the potential energy, and V is the volume of the nanowire for the purpose of averaging. Engineering strain is used as a measure of deformation and defined as $(l - l_0) / l_0$, where l is the instantaneous length of the wire and l_0 is the initial length of the wire obtained after the first step of energy minimisation corresponding to the initial configuration. The yield stress

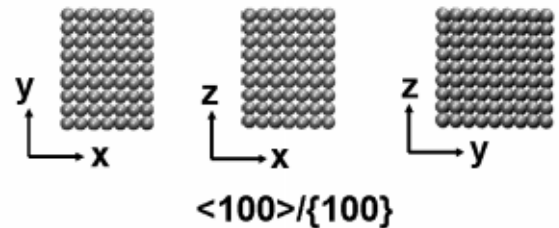


Figure 1. [100]/ {100} Copper nanowire with various orientations.

and the yield strain are found at the point of initial yield, that is, when the first defect which typically appears in the form of a partial dislocation, nucleates within the nanowires. Modulus of elasticity is calculated from the initial slope of the stress-strain curve for all the cases. The fracture strain is measured at the breaking point.

3. RESULTS AND DISCUSSIONS

3.1 Effect of Strain Rate

The effect of strain rate on the formation of pentagonal nanobridge structure under both the adiabatic and isothermal loading is discussed. Figures 2(a) and 2(b) show the stress-strain curve for a nanowire of cross-sectional dimension $0.723 \times 0.723 \text{ nm}^2$ at various strain rates of $1 \times 10^9 \text{ s}^{-1}$, $1 \times 10^8 \text{ s}^{-1}$, and $1 \times 10^7 \text{ s}^{-1}$ for isothermal and adiabatic thermal loading, respectively. Under isothermal loading, strain rate of $1 \times 10^9 \text{ s}^{-1}$ and $1 \times 10^7 \text{ s}^{-1}$ show the formation of pentagonal nanobridge structure, whereas no nanobridge structure is formed under the strain rate of $1 \times 10^8 \text{ s}^{-1}$ as shown in Fig.3(a). In the case of adiabatic loading, the formation of

nanobridge structure is observed at a strain rate of $1 \times 10^9 \text{ s}^{-1}$ and $1 \times 10^8 \text{ s}^{-1}$, whereas no nanobridge structure is formed under strain rate of $1 \times 10^7 \text{ s}^{-1}$ as shown in Fig. 3(b). Strain of 0.91 at a strain rate of $1 \times 10^8 \text{ s}^{-1}$ during adiabatic loading indicates that the increase in temperature during the tensile deformation of nanowires plays significant role in the formation of pentagonal nanobridge structure.

Mechanical properties, such as yield stress, yield strain, and modulus of elasticity of nanowires for a given cross-sectional dimensions are found to be same for both the adiabatic as well as isothermal loadings. It indicates that temperature does not play any role in the elastic properties of the nanowires at high strain rate. To confirm this, variation of temperature with respect to strain for various strain rates are shown in Fig. 4. Which shows a constant temperature till the yielding of the nanowires. Once yielding occurs, sudden rise in the temperature is observed which is due to the breaking of the bonds of the nanowires, which causes yielding to start. Similar behavior is also observed at the point of complete fracture of the nanowires. Sudden

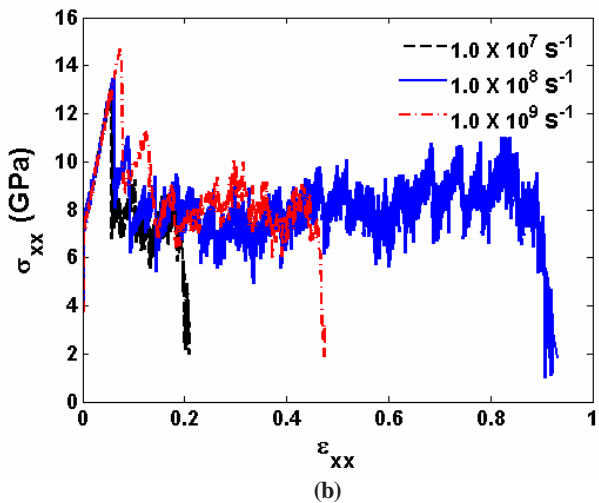
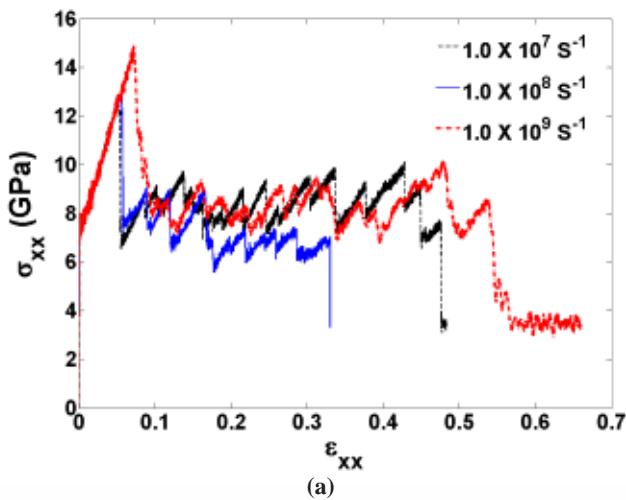


Figure 2. Stress-strain curve of [100]/ {100} copper nanowires of cross-sectional dimensions of $0.723 \times 0.723 \text{ nm}^2$ at various strain rates: (a) isothermal loading and (b) adiabatic loading.

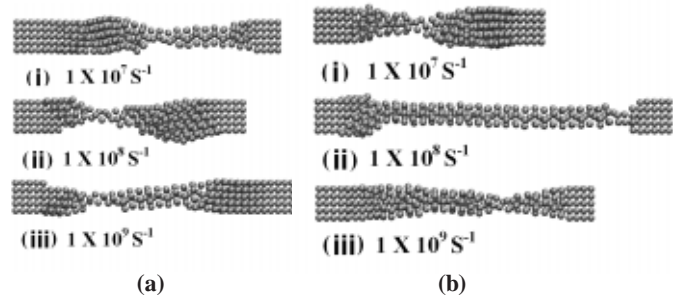


Figure 3. Deformed structure just before complete fracture of [100]/ {100} copper nanowires of cross-sectional dimensions of $0.723 \times 0.723 \text{ nm}^2$ an initial temperature of 10K with varying strain rate: (a) isothermal loading, and (b) adiabatic loading.

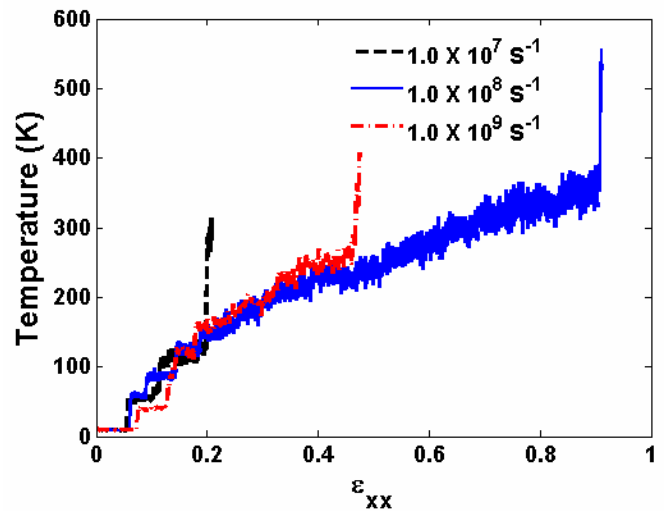


Figure 4. Variation of temperature versus strain of [100]/ {100} copper nanowires of cross-sectional dimensions of $0.723 \times 0.723 \text{ nm}^2$ at various strain rates during adiabatic loading.

increase in the temperature, and at the same time, sudden decrease in the strength of the nanowires are observed during complete fracture of the specimen, as shown in Fig. 4, for adiabatic loading condition. Decreasing yield stress and decreasing yield strain are observed with decreasing strain rate for a given cross-sectional dimensions of the nanowire for an initial temperature of 10K. Early yielding at a lower strain rate can also be seen in Fig. 4, where the jump in the temperature due to yielding occurred first for strain rate of $1 \times 10^7 \text{ s}^{-1}$ and subsequently higher yielding was observed with increasing strain rates. It is also observed that a given cross-sectional dimension and temperature with various strain rate loadings produce constant initial slope of the stress-strain curve as shown in Figs 2(a) and 2(b). This indicates a linear elastic and rate-insensitive response.

Different plastic deformations were observed for a given cross-sectional dimensions of nanowire with varying strain rates under adiabatic and isothermal loading. For example, $0.723 \times 0.723 \text{ nm}^2$ nanowire under the strain rate of $1.0 \times 10^8 \text{ s}^{-1}$ shows fracture strain of 0.34 under isothermal loading without formation of any nanobridge structure, whereas fracture strain of 0.91 is observed in the case of adiabatic loading with formation of a very long pentagonal nanobridge structure before fracture as

shown in Fig. 2(b). Strain rate of $1.0 \times 10^9 \text{ s}^{-1}$ shows formation of the pentagonal structure under both the thermal loading conditions as shown in Figs. 3(a) and 3(b). However, the fracture strains are found to be different; which is 0.55 for isothermal case and 0.48 for adiabatic case. The overall results show that the nanowire, which forms pentagonal nanobridge structure, can undergo more plastic deformation, but results can vary for different temperatures, cross-sections, and strain rates.

3.2 Effect of Nanowire Cross-sectional Size

In order to investigate the size effect, five different cross-sectional dimensions of the nanowires were considered, i.e. $0.723 \times 0.723 \text{ nm}^2$, $1.0845 \times 1.0845 \text{ nm}^2$, $1.446 \times 1.446 \text{ nm}^2$, $1.8075 \times 1.8075 \text{ nm}^2$, and $2.169 \times 2.169 \text{ nm}^2$. Figure 5 shows the stress-strain curves at a temperature of 10 K and strain rate of $1 \times 10^9 \text{ s}^{-1}$ [see Figs 5(a), and 5(b)] and $1 \times 10^8 \text{ s}^{-1}$ [see Figs 5(c), and 5(d)] for isothermal and adiabatic thermal loading, respectively. It is observed that various different thermal loading shows different inelastic deformations for a given strain rate and for a given cross-sectional area. For example, under a strain rate of $1 \times 10^9 \text{ s}^{-1}$, only the $0.723 \times 0.723 \text{ nm}^2$ cross-section forms a stable pentagonal nanobridge, when subjected to an isothermal condition. On the other hand, the cross-sectional dimensions of $0.723 \times 0.723 \text{ nm}^2$

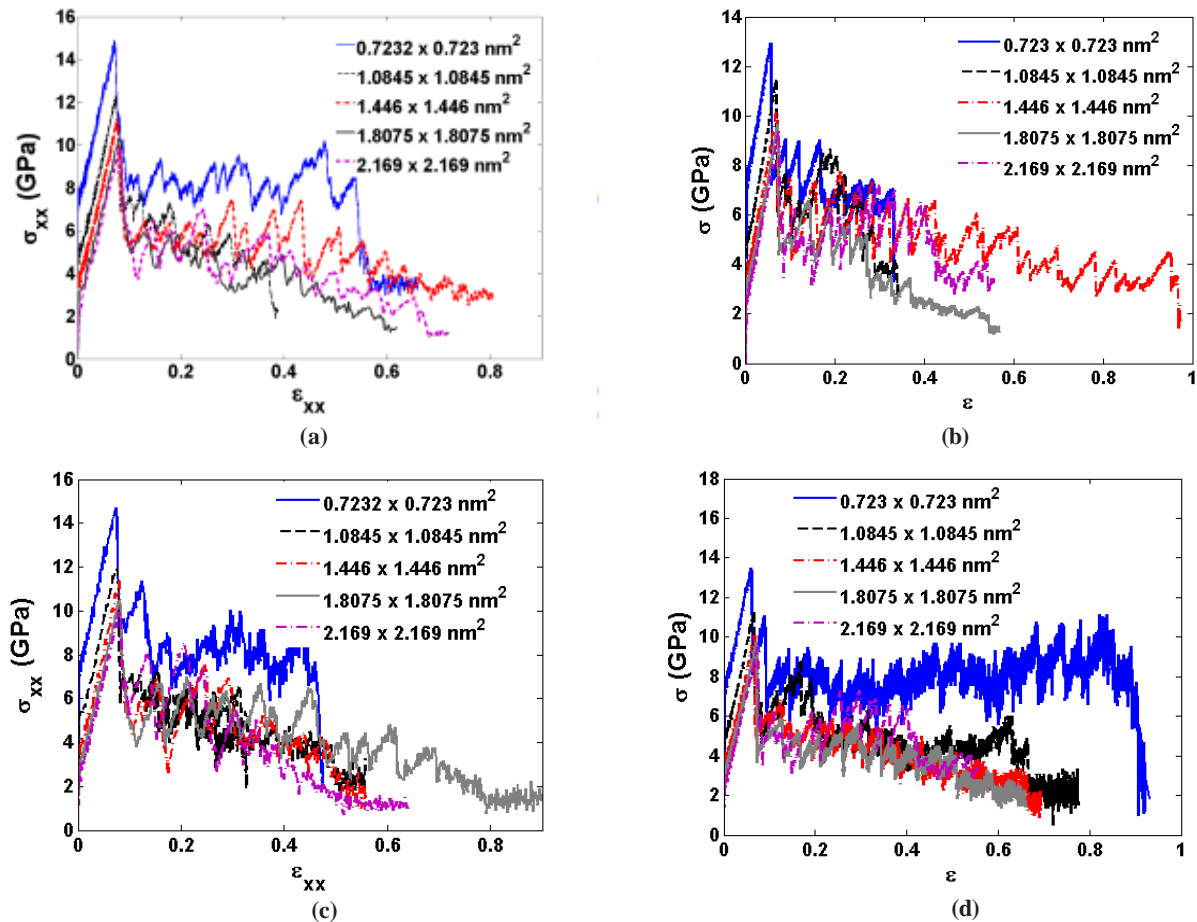


Figure 5. Stress-strain curves at 10 K for various cross-sectional dimensions of the copper nanowires: (a) and (b) for strain rate of $1 \times 10^9 \text{ s}^{-1}$; (c) and (d) for strain rate of $1 \times 10^8 \text{ s}^{-1}$; for isothermal and adiabatic loadings, respectively.

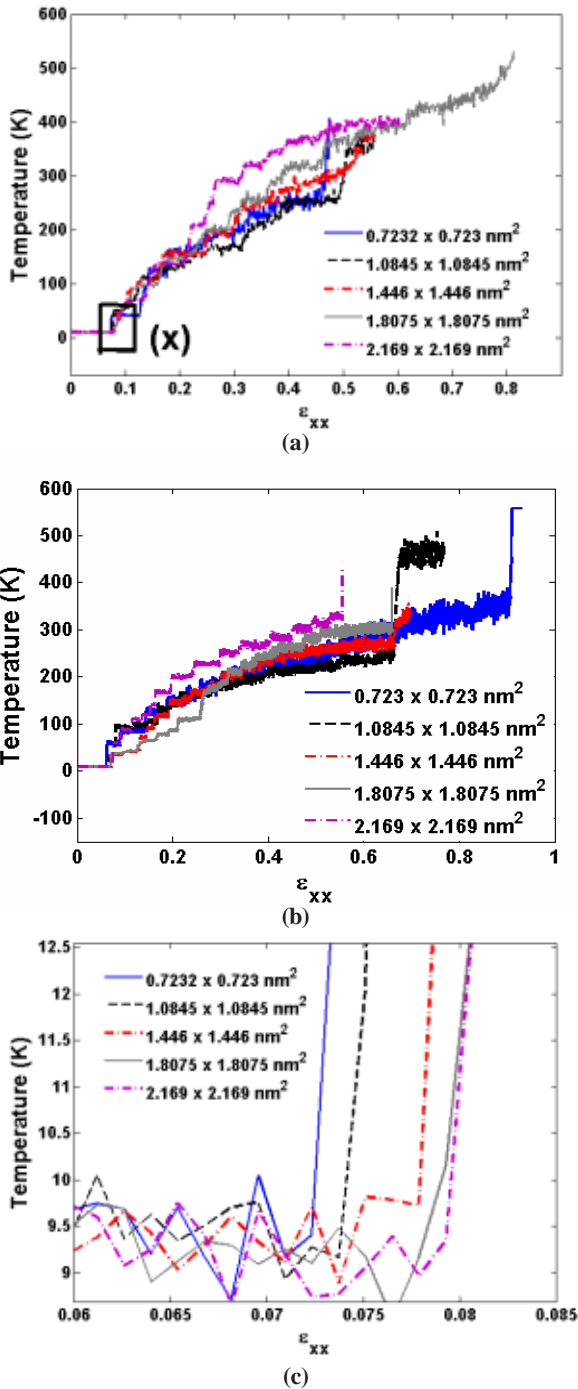


Figure 6. Variation of temperature versus strain during adiabatic loading of [100]/ {100} Cu nanowires of various cross-sectional dimensions at strain rates of (a) $1 \times 10^9 \text{ s}^{-1}$, (b) $1 \times 10^8 \text{ s}^{-1}$, (c) enlarged view of rectangular box marked as (x) in (a).

as well as $1.0845 \times 1.0845 \text{ nm}^2$ form such stable nanobridge structures, when subjected to adiabatic condition.

The mechanical properties, such as yield stress, yield strain and modulus of elasticity is found to be independent of both the adiabatic as well as the isothermal loading for a given strain rate of $1 \times 10^9 \text{ s}^{-1}$ with varying cross-sectional dimensions as shown in Figs 5(a), and 5(b), respectively.

A similar behaviour was also observed for reduced strain rate of $1 \times 10^8 \text{ s}^{-1}$ as shown in Figs 5(c), and 5(d) for isothermal and adiabatic loading, respectively. It also indicates that even with an increasing cross-sectional dimension of the nanowire, temperature does not play any role in the elastic properties of structure under high strain rate loading. Furthermore, to confirm this behavior, adiabatic temperature versus strain is plotted for varying cross-sectional dimension at strain rate of $1 \times 10^9 \text{ s}^{-1}$ and $1 \times 10^8 \text{ s}^{-1}$ as shown in Figs 6(a), and 6(b), respectively. These figures show that till yielding, no temperature change has occurred in the nanowire. An enlarged view of temperature variation for a given strain rate of $1 \times 10^9 \text{ s}^{-1}$ at yielding is shown in Fig 6(c). After yielding, a sudden jump in the temperature is observed in all the nanowires, which is due to the breaking of the bonds of the nanowires, which causes yielding to start. It is also observed that with an increasing cross-sectional dimensions, at the point of complete fracture, the magnitude of temperature jump is reduced. This is because, in the case of the thinner nanowires the strength decreases suddenly at the point of complete fracture, whereas in the case of larger cross-sections, the decrease in strength of the nanowire during plastic deformation is gradual, which can be seen in Fig 5. Figures 5(a), and 5(b) also show a constant slope of initial stress-strain curve for various cross-sectional dimensions at a strain rate of $1 \times 10^9 \text{ s}^{-1}$, whereas a rate-insensitive elastic modulus was already observed in Fig. 3. Hence, the overall response is due to a rate independent, thermal load independent, and cross-section independent elastic modulus of $\sim 100 \text{ GPa}$ before yielding. Decreasing yield stress and increasing yield strain are observed with an increase in the cross-sectional dimensions of the nanowire for a given strain rate and for both adiabatic as well as isothermal loading as shown in Fig. 7. Which also shows that with decreasing strain rate for a given cross-sectional dimension

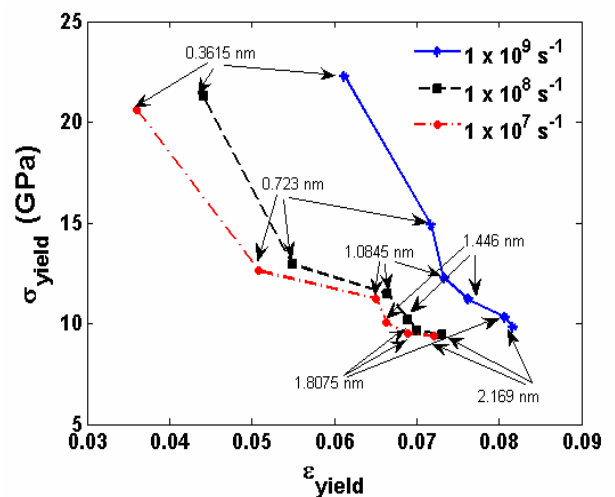


Figure 7. Yield stress-yield strain at various strain rates and cross-sectional dimensions of the copper nanowire, which is same for both the adiabatic as well as for isothermal loading for a given initial temperature of 10K.

of the nanowire, there are decreasing yield stress and decreasing yield strain.

4. CONCLUSIONS

A stable pentagonal multi-shell nanobridge structure during high strain rate tensile loading of [100]/ {100} constrained square cross-sectional copper nanowires under both the isothermal and adiabatic thermal loadings has been found. Such a stable structure has enhanced mechanical properties such as higher fracture strain. In addition, the pentagonal multi-shell structures were found to have an inherent stability that is dependent on the external loading rate applied to the nanowires. Strain rate insensitive, thermal load insensitive and cross-sectional dimension insensitive elastic modulus of ~ 100 GPa is also found. Decreasing yield stress and decreasing yield strain have been observed with decreasing strain rate for a given cross-sectional dimensions of the nanowires under both the thermal loading cases. For a given strain rate with increasing cross-sectional area, a decreasing yield stress and an increasing yield strain are also observed. It is also found that the adiabatic thermal loading does not change elastic properties of the nanowire under such high strain rate loading at an initial temperature of 10K. Different plastic deformations have been observed for both the isothermal as well as adiabatic loadings, which is an indication that processing temperature can lead to different inelastic deformations for a given strain rate under different thermal loadings.

ACKNOWLEDGEMENTS

Vijay Kumar Sutrarak thanks R. Raghunathan, Group Director, and C.M. Venkatesh, Head of Mechanical Engineering Design Division, Aeronautical Development Establishment, Bangalore, for their positive support and encouragement during this research work.

REFERENCES

1. Wang, B.; Yin, S.; Wang, G.; Buldum, B. & Zhao, J. Novel structures and properties of gold nanowires. *Phys. Rev. Lett.*, 2001, **86**, 2046.
2. Bilalbegovic, G. Structure and stability of finite gold nanowires. *Phys. Rev.*, 1998, **B 58**, 412.
3. Tosatti, E.; Prestipino, S.; Kostlmeier, S.; Dal Corso, A. & Di Tolla, F. D. String tension and stability of magic tip-suspended nanowires. *Science*, 2001, **291**, 288.
4. Bilalbegovic, G. Structures and melting in infinite gold nanowires. *Solid State Commun.*, 2000, **115**, 73.
5. Torres, J. A.; Tosatti, E.; Dal Corso, A.; Erolessi, F.; Kohanoff, J. J.; Di Tolla, F. D. & Soler, J. M. The puzzling stability of monatomic gold wires. *Surf Sci.*, 1999, **426**, L441.
6. Bilalbegovic, G. Metallic nanowires: multi-shelled or filled. *Comput. Mater Sci.*, 2000, **18**, 333.
7. Hwang, H. J. & Kang, J. W. *J. Korean Phys. Soc.*, 2002, **40**, 283.
8. Kang, J. W. & Hwang, H. J. An atomistic simulation study of cylindrical ultrathin Cu nanowires. *Mol. Simul.*, 2002, **28**, 1021.
9. Kang, J. W. & Hwang, H. J. Pentagonal multi-shell Cu nanowires. *J. Phys.: Condens. Matter*, 2002, **14**, 2629-636
10. Gulseren, O.; Erolessi, F. & Tosatti, E. Pentagonal multi-shell Cu nanowires. *Phys. Rev. Lett.*, 1998, **80**, 3775.
11. DiTolla, F.; Dal Corso, A.; Torres, J. A. & Tosatti, E. Electronic properties of ultra-thin Aluminum nanowires. *Surf Sci.*, 2000, **456**, 947.
12. Gulseren, O.; Erolessi, F. & Tosatti, E. Premelting of thin wires. *Phys. Rev.*, 1995, **51**, 7377.
13. Finbow, G. M.; Lyden-Bell, R. M. & McDonald, I. R. Atomistic simulation of the stretching of nanoscale metal wires. *Mol. Phys.*, 1997, **92**, 705.
14. Wang, B.; Yin, S.; Wang, G. & Zhao, J. Structures and electronic properties of ultrathin titanium nanowires. *J. Phys.: Condens. Matter*, 2001, **13**, L403.
15. Diao, J. & Gall, K. Surface-stress-induced phase transformation in metal nanowires. *Nature Materials*, 2003, **2**, 656-660.
16. Kondo, Y. & Takayanagi, K. A. Model of Direct Gauge Mediation of Supersymmetry Breaking. *Phys. Rev. Lett.*, 1997, **79**, 18.
17. Diao, J. & Gall, K. Surface stress driven reorientation of gold nanowires. *Phys. Rev.* 2004, **70**, 075413.
18. Lieber, C. M. Nanoscale science and technology: building a big future from small things. *MRS Bulletin*, 2003, **28**, 7.
19. Patolsky, F. & Lieber, C. M. Nanowire nanosensors. *Materials Today*, 2005, **8**, 4.
20. Huang, M. H. & Mao, S. Room-temperature ultraviolet nanowire nanolasers. *Science*, 2001, **292**, 5523.
21. Dual, X. & Huang, Y. Single-nanowire electrically driven lasers. *Nature*, 2003, **421**, 241- 45.
22. Arnold, M. S. & Avouris, P. Field-effect transistors based on single semiconducting oxide nanobelts. *J. Phys. Chem.*, 2003, **B107**, 659-63.
23. Wu, Y. & Xiang, J. Single-crystal metallic nanowires and metalsemiconductor nanowire heterostructures. *Nature*, 2004, **430**, 61-64.
24. Duan, X. & Hunag, Y. Single-nanowire electrically driven lasers. *Nature*, 2003, **409**, 66-69.
25. Terabe, K. & Hasegawa, T. Quantized conductance atomic switch. *Nature*, 2005, **433** 47-50.
26. Walter, E.C. & Penner, R.M. Sensors from electrodeposited metal nanowires. *Surf. Interface Anal.*, 2002, **34**, 409-12.
27. Comini, E. & Faglia, G. S. Stable and highly sensitive gas sensors based on semiconducting oxide nanobelts. *Appl. Phys. Lett.*, 2002, **81**, 10.
28. Cui, Y. & Wei, Q. Nanowire nanosensors for highly sensitive and selective detection of biological and chemical species. *Science*, 2001, **293**, 5533.
29. Zhong, Z. & Wang, D. Nanowire crossbar arrays as address decoders for integrated nanosystems. *Science*,

- 2003, **302**, 5649.
30. Lieberman, D.S. & Wechsler, M.S. Cubic to orthorhombic diffusionless phase change; experimental and theoretical studies of *AuCd*. *J. Appl. Phys.*, 1955, **26**, 4.
 31. Stalder, A. & Durig, U. Study of yielding mechanics in nanometer-sized Au. *Appl. Phys. Lett.*, 1995, **68**, 5.
 32. Kondo, Y. & Takayanagi, K. Synthesis and characterization of helical multi-shell gold nanowires. *Science*, 2000, **289**, 5479.
 33. Konishi, Y. & Motoyama, M. Electrodeposition of Cu nanowire arrays with a template. *J. Electroanalytical Chem.*, 2003, **559**, 149-53.
 34. Michaelian, K.; Rendon, N. & Garzon, I. L. Structure and energetics of Ni, Ag, and Au nanoclusters. *Phys. Rev.*, 1999, **B60**, 2000.
 35. Erkoc, S. Stability of gold clusters: molecular-dynamics simulations. *Physica*, 2000, **E8**, 210.
 36. Li, T. X.; Yin, S. Y.; Ji, Y. L.; Wang, B. L.; Wang, G. H. & Zhao, J. J. A genetic algorithm study on the most stable disordered and ordered configurations of Au 38-55. *Phys. Lett.*, 2000, **A267**, 403.
 37. Catlow, C. R. A.; Bulatov, V. L. & Grimes, R. W. Computational studies of structures, energetics and dynamics of clusters. *Nucl. Instrum, Methods Phys. Res.*, 1997, **B122**, 301
 38. Rongwu, L.; Zhengying, P. & Yukun, H. Molecular-dynamics simulations of slow copper cluster deposition. *Phys. Rev.*, 1996, **B53**, 4156.
 39. Lammers, U. & Borstel, G. Electronic and atomic structure of copper clusters. *Phys. Rev.*, 1994, **B49**, 17360.
 40. Mehrez, H. & Ciraci, S. Yielding and fracture mechanisms of nanowires. *Phys. Rev.*, 1997, **B56**, 12632.
 41. Sen, P.; Gulseren, O.; Yildirim, T.; Batra, I.P. & Ciraci, S. A first-principles study of the atomic and electronic Pentagonal nanowires. *Phys. Rev.*, 2002, **B65**, 235433-1.
 42. Gonzalez, J.C., Rodrigues, V.; Bettini, J.; Rego, L.G.C.; Rocha, A.R.; Coura, P.Z., Dantas, S.O.; Sato, F., Galvao, D.S. & Ugarte, D. Indication of unusual pentagonal structures in atomic-size Cu nanowires. *Phys. Rev. Lett.*, 2004, **93**, 126103-1
 43. Sutrar, Vijay Kumar. & Mahapatra, D. Roy. Formation of stable ultra-thin Pentagon Cu nanowire under high strain rate loading. *J. Phys.: Condens. Matter*, 2008, **20**, 335206.
 44. Sutrar, Vijay Kumar. & Mahapatra, D. Roy. Coupled effect of size, strain rate, and temperature on the shape memory of a pentagonal Cu nanowire. *Nanotechnology*, 2009, **20**, 045701.
 45. Sutrar, Vijay Kumar. & Mahapatra, D. Roy. An Ultra-Stable Cu Nanowire under Thermo-Mechanical Loading: A Molecular Dynamic Study. *In Int. Conf. Smart Material, Structures and Systems (ISSS-08)*, IISc, Bangalore, India, 2008.
 46. Daw, M. S. & Baskes, M. I. Embedded-atom method: Derivation and application to impurities, surfaces, and other defects in metals. *Phys. Rev.*, 1984, **B29**, 6443-453.
 47. Daw, M. S.; Foiles, S. M. & Baskes, M. I. The embedded-atom method-a review of theory and applications. *Mater. Sci. Rep.*, 1993, **9**, 251-310.
 48. Mishin, Y.; Mehl, M.; Papaconstantopoulos, D. A.; Voter, A. F. & Kress, J. D. Structural stability and lattice defects in copper: *Ab initio*, tight-binding, and embedded-atom calculations. *Phys. Rev.*, 2001, **B63**, 224106.
 49. Nose, S. A. Unified formulation of the constant temperature molecular dynamics methods. *J. Chem. Phys.*, 1984, **81**, 511-9.
 50. Hoover, W. G. Canonical dynamics: equilibrium phase-space distributions. *Phys. Rev.*, 1985, **A31**, 1695-7.
 51. Liang, W. & Zhou, M. *Nanotech 2*. 2003 www.nsti.org, ISBN 0-9728422-1-7.
 52. Swope, W. C.; Anderson, H. C.; Berens, P. H. & Wilson, K. R. A. Computer simulation method for the calculation of equilibrium constants for the formation of physical clusters of molecules: application to small water clusters. *J. Chem. Phys.*, 1982, **76**, 637-649.
 53. Plimpton, S. J. Fast parallel algorithms for short-range molecular dynamics. *J. Comput. Phys.*, 1995, **117**, 1-19.
 54. LAMMPS 2007 <http://www.cs.sandia.gov/~sjplimp/lammps.html>
 55. Zhou, M. A new look at the atomic level virial stress: on continuum-molecular system equivalence. *Proc. Royal Soc.*, 2003, **A459**, 2347-392.

Contributors



Mr Vijay Kumar Sutrar received his BE (Mech Engg) from Government Engineering College, Rewa, M.P. in 2002 and MTech (Design Engg) from Indian Institute of Technology, New Delhi, in 2004. He joined DRDO in 2004 at ADE as Scientist B. Presently, he is working as Scientist C in Mechanical Engineering Design Division of Aeronautical Development Establishment, DRDO, Bangalore. He is also pursuing PhD in structures stream from IISc, Bangalore. His area of interest includes finite element modelling and analysis of aircraft structures, fatigue and fracture mechanics, Molecular dynamics simulations of nanomaterials, and designing of nanomaterials for high temperature and high strength applications.



Mr D. Roy Mahapatra is currently an Assistant Professor at the Indian Institute of Science, Bangalore. He obtained BE (Civil Engg) from Jadavpur University in 1998 and PhD in Aerospace Engineering from IISc, Bangalore, in 2004. During 2005-2006, he was a NSERC postdoctoral fellow in applied mathematics in Canada. Since 2006, he has been with IISc Bangalore. His research interests are in

the areas of integrative systems with sensors and actuators,

multiscale and multifunctional materials, micro and nanoengineering, mechanics of materials, phase transformation with application to smart materials, dynamics and control of distributed parameter systems, wave propagation. He has published more than 70 international journal papers and more than 60 international conference papers. He is coauthor of an advanced graduate text book on Spectral Finite Element Method. He currently leads a multidisciplinary research group of 15 graduate student and project staff and the Integrative Multiscale Engineering Materials and Systems Lab at the Department of Aerospace Engineering, IISc Bangalore.